Field evolution of the magnetic normal modes in elongated permalloy nanometric rings



2007 J. Phys.: Condens. Matter 19 406229

(http://iopscience.iop.org/0953-8984/19/40/406229)

IOP PUBLISHING JOURNAL OF PHYSICS: CONDENSED MATTER

J. Phys.: Condens. Matter **19** (2007) 406229 (12pp) doi:10.1088/0953-8984/19/40/406229

# Field evolution of the magnetic normal modes in elongated permalloy nanometric rings

**G Gubbiotti[1,7], M Madami[1], S Tacchi[1], G Carlotti[2,3], M Pasquale[4], N Singh[5], S Goolaup[6] and A O Adeyeye[6]**

[1] CNISM, Dipartimento di Fisica, Università di Perugia, Via A Pascoli, I-06123 Perugia, Italy
[2] Research Center S3-INFM-CNR, Via Campi 213/a, 41100, Modena, Italy
[3] Dipartimento di Fisica, Universita' di Perugia, Via A Pascoli, 06123 Perugia, Italy
[4] Istituto Nazionale di Ricerca Metrologica, Strada delle cacce 91, 10135 Torino, Italy
[5] Institute of Microelectronics, 11 Science Park Road, Singapore Science Park II, 117685, Singapore
[6] Information Storage Materials Laboratory, Department of Electrical and Computer Engineering, National University of Singapore, 4 Engineering drive 3, 117576, Singapore

E-mail: gubbiotti@fisica.unipg.it

Received 11 July 2007, in final form 12 July 2007
Published 21 September 2007
Online at stacks.iop.org/JPhysCM/19/406229

**Abstract**

The eigenmode spectrum of elongated permalloy rings with relatively wide arms is investigated by combined Brillouin light scattering and ferromagnetic resonance measurements as a function of the applied field intensity, encompassing both vortex and onion ground states. To reproduce the frequencies and the spatial profiles of the measured modes we performed micromagnetic simulations which solve the discretized Landau–Lifshitz–Gilbert equation in the time domain and calculate locally the Fourier transform. This allowed us to correlate the field dependence of different modes to their localization inside different portions of the rings. With the rings in the vortex ground state, in addition to radial, fundamental, and azimuthal modes, a localized mode, existing in the element portions where the internal field assumes its minima, has been measured and identified. This latter mode, whose frequency decreases for increasing field intensity, becomes soft near the transition from vortex to onion state and determines the change in symmetry of the magnetic ground state. After the transition, it is replaced by two edge modes, localized on the internal and external boundary of the rings, respectively.

(Some figures in this article are in colour only in the electronic version)

## Introduction

Nanomagnetic elements with ring shape have attracted considerable attention during the last few years because of the unique magnetization distribution, namely the vortex state, in which

[7] Author to whom any correspondence should be addressed.

the magnetization is circumferential, and the onion state with two opposite head-on (180°) domain walls [1]. For their unique stable magnetization configurations, ring elements have been proposed as a candidate for magnetic random access memory [2–4]. Several authors have investigated the switching mechanism and its dependence on the geometrical parameters such as the film thickness, the ring width and the ring diameter [5, 6]. While most of the studies were devoted to investigating the static properties of circular rings, a very small number was focused on asymmetric rings. Castaño *et al* [7] investigated the magnetization reversal process exhibited by elliptical-ring-shaped magnets using magnetic-force microscopy and micromagnetic simulations. Particular attention has been devoted to the anisotropic behaviour induced by the ellipticity of the rings which creates different magnetization reversal mechanisms, depending on the applied field direction. Saitoh *et al* [8] have shown that it is possible to control the direction of magnetic moment circulation in off-centred $Ni_{81}Fe_{19}$ rings. Mani and co-workers [9] analysed the switching mechanism in square and rectangular rings using magnetic-force microscopy and found that they exhibit two stable states of opposite polarity at remanence, while the switching mechanism can be controlled by the ring geometry. Adeyeye *et al* [10] demonstrated the possibility of stabilizing the two magnetic states in elongated permalloy nanorings, demonstrating the crucial role of thickness in the range between 5 and 60 nm.

In addition to the study of the static magnetization configuration, more recently a large amount of work has been devoted to probing magnetic excitations in thin circular rings in both the vortex and the onion state. New effects, such as mode-splitting or negative frequency versus field dependence, have been observed by ferromagnetic resonance (FMR) [11–13] and Brillouin light scattering (BLS) experiments [14]. In the latter work, using an interpretation scheme based on the dynamic matrix approach and the evaluation of the BLS cross-section, it was possible to identify all the relevant magnetic excitations of nanometric rings. It was also shown that, starting from the vortex ground state, as soon as the applied field is switched on, localization effects occur for all the modes. Each radial mode splits into two modes, localized in opposite arms of the ring, whose frequency either increases or decreases, depending on the different values of the internal field experienced by the precessing spins.

In this paper the results of a combined BLS and FMR analysis of 10 nm thick elongated permalloy rings, with a small elliptical hole, is reported. The choice of such an unusual shape of the rings, characterized by a relatively large width of the arms, is motivated by the fact that a moderate external field causes a marked distortion of the vortex ground state with the appearance of noticeable inhomogeneity of the internal magnetic field. This is quite different from the previously studied case of circular rings characterized by a small width, where the internal field profile is much more regular and smooth. A major aim of this paper is therefore to investigate how the inhomogeneity of the internal field affects the properties of the magnetic eigenmodes. Their frequencies have been measured as a function of the applied magnetic field $H$ in the range between 0 and 500 Oe, encompassing both the vortex and onion states. The experimental results are compared to micromagnetic simulations, enabling us to reveal the spatial distribution of the modes and their evolution with the applied field, with emphasis given both to localization effects and to the role of dynamical modes in assisting the transition from vortex to onion ground state.

## 1. Samples and experimental techniques

Large area ($4 \times 4$ mm$^2$) arrays of 10 nm thick asymmetric elongated $Ni_{80}Fe_{20}$ rings with elliptical holes were fabricated on silicon substrates using a 248 nm deep ultra-violet lithography exposing wavelength [10, 15]. The long (short) axis length of the ring is 780 nm

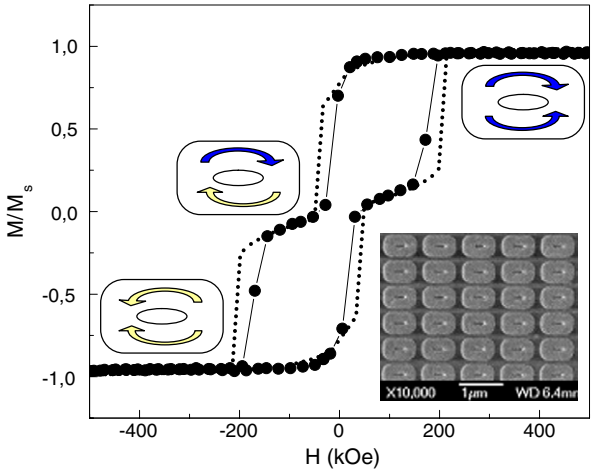


**Figure 1.** Measured (full dots) and calculated (dotted line) longitudinal hysteresis loop when the external field is applied along the long axis of the rings (easy magnetization direction). The arrows indicate the sense of circulation of the magnetization in the two halves of the ring. The inset contains the SEM image of the ring array.

(490 nm), while the long (short) axis of the elliptical hole is 203 nm (55 nm). The inter-ring spacings along the major and minor axes are 160 and 125 nm, respectively. A scanning electron microscopy (SEM) image of the ring array is shown in the inset of figure 1 and reveals the good morphology of the pattern as far as both the uniformity and the dimensional control of the shape and periodicity are concerned. Longitudinal magneto-optic Kerr effect magnetometry (MOKE) was used to measure the hysteresis loop of the rings.

BLS experiments were performed in the backscattering configuration using a Sandercock-type (3+3)-pass tandem Fabry–Perot interferometer. A reversible dc magnetic field was applied along the in-plane easy direction of the rings and perpendicularly to the incidence plane of light. The spectra were recorded starting from a bias field $H = 0$ Oe, with the ring in the vortex state, up to 500 Oe, where the rings are almost completely saturated.

The microwave behaviour of the sample was characterized using a commercial 50 Ω matched coplanar waveguide connected to an Anritsu 40 MHz–65 GHz vector network analyser (VNA) through end-launch connectors. The samples were positioned face down on the centre of the coplanar waveguide and with the easy magnetization axis parallel to the propagation direction. The waveguide was inserted in the gap of an electromagnet, producing a field up to 5 kOe along the centre conductor direction. After a proper calibration of the VNA using a standard SOLT procedure, the film characterization consisted of repeated measurements of the scattering matrix $S$ from 40 MHz to 30 GHz, under different values of the applied bias field and different field histories. The $S$ matrix data were then analysed offline. The frequencies of the main FMR peak and the associated line-width were determined by the real and imaginary parts of the normalized permeability [16], which was obtained by comparing $S$ parameter spectra measured under different values of the applied dc field.

## 2. Normal mode simulations

The numerical 2D OOMMF micromagnetic package (version 1.2.0.4) [17] was used to simulate both the static magnetization configuration and the dynamical properties of the ring, which was

discretized into cells of dimensions $5 \times 5 \times 10\ \text{nm}^3$. We neglect variations of the magnetization perpendicular to the element plane ($z$-direction) due to the small thickness of the layers. The magnetic parameters used for polycrystalline permalloy are $M_s = 700 \times 10^3\ \text{A m}^{-1}$ for the saturation magnetization, $A = 8 \times 10^{-13}\ \text{J m}^{-1}$ for the exchange stiffness constant and $\gamma = 2.9\ \text{GHz kOe}^{-1}$ for the gyromagnetic ratio. These magnetic parameters were derived from the BLS investigation of the unpatterned permalloy film having the same thickness of the rings, which was used as a reference sample. Magnetocrystalline anisotropy was neglected and the rings were considered as non-interacting. This assumption is motivated by the fact that when the rings are in the vortex state the dipolar stray field is negligible, and even for elements in the saturated state the dipolar coupling becomes experimentally sizable for inter-element separation below about 100 nm only [18].

As far as the dynamical calculations are concerned, here we briefly recall the procedure for calculating the eigenmode frequencies and profiles, while a complete description is found in [19–21]. For each applied field, the equilibrium magnetization distribution is used as the starting magnetic ground state and the system is excited by a short out-of-plane Gaussian field pulse with peak amplitude of 10 Oe and full width at half maximum of 2 ps. To excite all the magnetic eigenmodes, which are characterized by different spatial symmetries, the field pulse is built from the superposition of a uniform pulse and a pulse localized in the upper half of the ring. The time evolution under the Landau–Lifshitz–Gilbert (LLG) equation of the magnetization has been recorded for each computational cell at regular time steps ($\Delta t = 5$ ps) and with a damping factor set to $\alpha = 0.01$. The overall power spectrum, with a frequency resolution of 0.2 GHz, is finally obtained by summing the local power spectrum of the whole set of cells. To reduce the calculation time we used a fifth-order Runge–Kutta integrator (rkf54s) with an error rate parameter of $1 \times 10^{-7}$, which is faster and more accurate than the Euler evolver [17]. The 2D spatial distribution of each eigenmode is achieved by plotting either the real or the imaginary part of the Fourier coefficients for each eigenfrequency[8]. In reporting these mode profiles we plot the component of the magnetization vector which is perpendicular to the sample plane ($m_z$), because it gives the main contribution to the BLS cross-section [22].

According to the previous literature, when the rings are in the vortex and onion ground states, the classification of the magnetic eigenmodes is similar to the case of disks and continuous magnetic film, respectively [23]. In the vortex case, the modes are azimuthal $(m, 0)$ and radial $(0, n)$, where the $m$ and $n$ integers specify the number of nodal lines of the dynamic magnetization perpendicular and parallel to the magnetization. The fundamental mode (F) without nodal lines corresponds to the Kittel uniform mode [24]. In the onion state, the mode labels are derived from the eigenmode classification in a continuous magnetic film, see [23], where (i) EM denotes the edge modes, i.e. the modes that are localized near the particle edges in the direction of the applied magnetic field, (ii) $m$-BA denotes the dipolar modes with nodal lines perpendicular to $H$ (backward-like modes), and (iii) $n$-DE stands for modes with nodal lines parallel to the direction of $H$ (Damon–Eshbach-like modes). The 'mixed' modes (iv) are labelled $m$-BA $\times$ $n$-DE.

[8] Note that both the real and the imaginary parts of the coefficients describe the same mode and have the same symmetry. However, the relative amplitude of the two components is different for the various modes, so in figure 4 we have plotted for each mode the largest component. In this respect, it interesting to observe that for those modes which represent a resonance of the whole dot (such as the F or the DE modes) the imaginary part prevails, in agreement with the well known fact that the susceptibility of an oscillating system would be imaginary at resonance. Please note that our approach gives similar results to the method reported in [20, 21], where the spatial distribution of the modes is obtained by plotting the square of the amplitude of the Fourier coefficients, but has the advantage that information about the nodal planes of the modes is not missed.

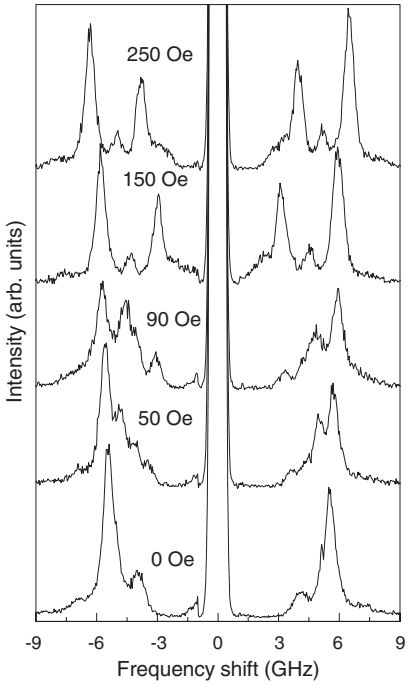


**Figure 2.** Sequence of Brillouin light scattering spectra for different values of the magnetic field $H$ applied along the ring's long axis.

## 3. Results and discussion

The hysteresis curves measured (full dots) and calculated (dotted line) with a magnetic field applied along the rings major axis are shown in figure 1. Starting from $H = 500$ Oe, which saturates the magnetization of the rings, the field was swept toward $H = -500$ Oe at constant steps of 10 Oe. In the branches of the magnetization curve we observed two discontinuities associated with the transitions from onion to vortex state and vice versa, as the applied field $H$ is swept from positive to negative saturation. The observed magnetization plateau, about 100 Oe wide, corresponds to the configuration where the vortex state is stable. The shape of the measured loop was satisfactorily reproduced by micromagnetic simulations even if the switching fields were slightly overestimated (the calculated value of the vortex-to-onion transition is 203 Oe, instead of the experimental value of about 150 Oe). This is possibly due to the fact that the discretization with cubic cells fails to reproduce the details of both the hole shape and the surface roughness of the real elements. In addition, the simulations are carried out at $T = 0$ K, so that thermal activation of the switching is ignored.

To generate the vortex state for the BLS measurements, the rings were saturated with a positive applied field, which was then reduced to zero and reversed down to $-100$ Oe, where the rings are in the vortex state, as discussed above. From there, the field was increased to positive values and the BLS spectra were recorded at regular intervals.

A sequence of BLS spectra recorded for different values of the applied field $H$ is shown in figure 2. We notice the presence of several well resolved peaks, whose number increases as soon as the applied field is switched on. In particular, the peaks detected at 4 and 5.5 GHz for $H = 0$ split into a doublet of new peaks having a direct and inverse field dependence, respectively. To

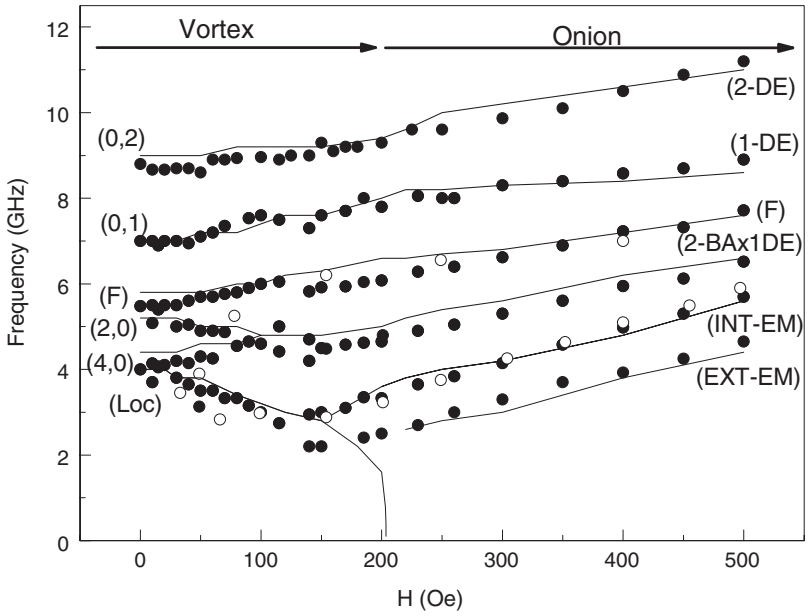


**Figure 3.** Experimental frequencies measured by BLS (full dots) and by FMR (open dots) as a function of the magnetic field $H$ from 0 Oe up to 500 Oe. The curves represent the frequencies calculated by the micromagnetic calculations. The field ranges of the vortex and onion ground states, derived from simulations, are indicated by the arrows.

obtain a clear picture of the mode behaviour, in figure 3 we plot the field dependence of the spin modes measured by both the BLS (full dots) and the FMR technique (open dots). The observed FMR frequencies are in fairly good agreement with the BLS results, although only a couple of modes was detected by FMR, due to limitations in the coupling between the coplanar line and the very thin sample, which was just positioned (and not micro-fabricated) on top of the waveguide [25]. In this respect, it will become clear in the following that the modes detected by FMR in the above mentioned weak-coupling conditions tend to be associated with large and spatially uniform $m_z$ components, which are able to perturb the signal transmission along the waveguide and also give rise to the largest BLS signal intensity.

In order to fully understand the field evolution of the measured modes, we have calculated the static magnetization distribution (first row of figure 4) and the internal magnetic field $H_{\rm int}$, defined as the sum of the Zeeman and magnetostatic fields (second row of figure 4), as well as the mode profiles (lower rows of figure 4) for four different values of the applied field $H$. A more detailed and quantitative analysis of the values of $H_{\rm int}$ along a rectangular path ABCD within the ring is also reported in figure 5 for the same values of $H$.

First of all we notice that, contrary to the case of circular rings [14], for $H = 0$ the internal field is not always zero, due to the combined effect of the elongated shape of the elements and of the quite large width of the ring arms. However, referring to the rectangular path ABCD in figure 5, $H_{\rm int}$ vanishes along the BC and DA segments, where $M$ and $H$ are either parallel or antiparallel. In addition, along the rectangular path there are four regions (close to the corners) where the internal field presents its minima. It will be shown that in these regions several modes present a large oscillation amplitude of the dynamical magnetization, since for small values of the internal field the effective field (sum of the internal and exchange fields) experienced by the precessing spins is also small, so the spins are free to rotate with a large transversal magnetization amplitude.

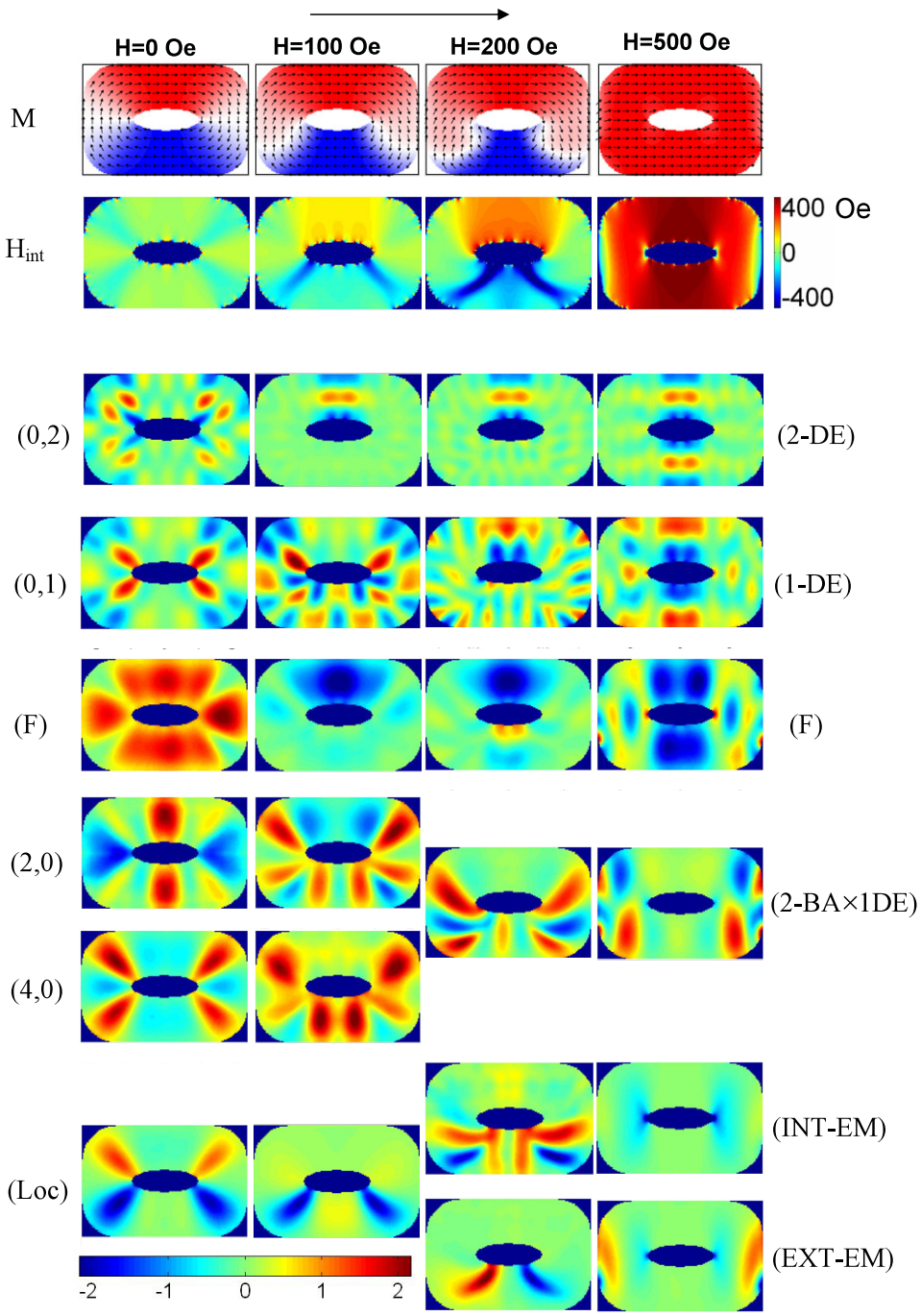


**Figure 4.** Static magnetization configurations ($M$, first row) and internal magnetic field profiles ($H_{\text{int}}$, second row) calculated for the rings at different values of the externally applied field, from zero (vortex state) to 500 Oe (onion state). The field direction is indicated by the arrow and the white regions correspond to a perpendicular orientation between $M$ and $H$. Lower rows: calculated spatial distribution of the $m_z$ magnetization component for different modes observed in the BLS spectra at the field values indicated on the top of the figure.

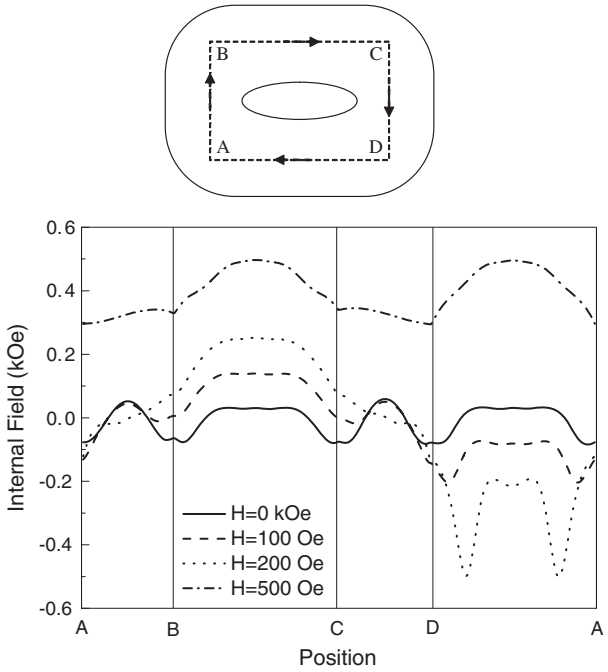


**Figure 5.** Calculated values of the internal magnetic field ($H_{\text{int}}$) along a closed rectangular path ABCD for different values of the externally applied field $H$.

Let us now discuss in more detail the evolution of both the frequency and the spatial distribution of the modes as a function of the external field. This description is based on the results of the micromagnetic calculation, which, as already mentioned at the beginning of this paragraph, slightly overestimates the vortex–onion transition field with respect to the experimental one.

### *3.1. Vortex state at $H = 0$*

For $H = 0$ the rings are in the vortex ground state and most of the modes have profiles similar to those found in the case of circular rings [14]. Starting from the highest frequency, we observe a couple of radial $(0, n)$ modes, the fundamental mode (F), which exhibits the largest intensity in the BLS spectra, and the azimuthal $(m, 0)$ modes. Some of the modes, like the F and the $(2, 0)$, have large oscillation amplitude in the ring regions where the internal field is almost uniform, i.e. corresponding to the central parts of the arms. In contrast, the modes $(0, 2)$, $(0, 1)$, and $(4, 0)$ present their maxima corresponding to the minima of the internal field (i.e. at the A, B, C, and D points). Remarkably, a low-frequency mode is also found (labelled Loc), which is completely localized just in the above mentioned A, B, C, and D minima. The existence of the latter mode, in particular, is a novelty with respect to circular rings in the vortex state [14], because its localization is strictly connected to the inhomogeneity of the internal field due to the quasi-rectangular shape of the present elements.

### *3.2. Distorted vortex state ($0 < H < 203$ Oe)*

When the external field $H$ is switched on, the frequency of all the modes is substantially constant until $H$ does not exceed about 50 Oe, because the applied field does not modify

significantly the vortex ground state. Then, the frequency of both the fundamental and the radial modes increases with $H$. This happens because when $H$ is increased all these modes become localized in the upper part of the ring (where $M$ and $H$ are parallel). Here the internal field is always positive, as shown in figure 5, and this accounts for their frequency increase. This is different from the previous results relative to thin circular rings [14], where the radial modes exhibited a splitting, with either positive or negative frequency slopes, depending on their localization within the upper or the lower arm of the ring, respectively. In the present case no radial modes with negative frequency slope are observed in the spectra, because the rectangular shape of the dots and the larger ratio between external and internal radii inhibits the localization of such modes in the lower arm. This can be understood looking at the profiles of the magnetization and of the internal field for $H = 100$ and 200 Oe, in figures 4 and 5. It is clear that in the lower arm (D–A in figure 5) the internal field is far from being uniform, presenting two deep minima, thus preventing the existence of modes with the same spatial symmetry found in the upper arm (B–C in figure 5), where the internal field is roughly uniform.

A more complex behaviour is observed for azimuthal modes; in particular, the mode $(2, 0)$ has a negative field dependence on the applied field strength, while the opposite occurs for the $(4, 0)$ one. Again, this different behaviour can be comprehended looking at the evolution of the internal field and of the ring portions where these modes are localized: on increasing the external field from zero, the $(2, 0)$ mode leaves the regions where $H_{\text{int}}$ was vanishing and occupies regions (positions B and C, as well as the lower ring arm) where the internal field is negative. In contrast the $(4, 0)$ mode, which for $H = 0$ was localized in the four minima of the internal field, now occupies regions with less negative or zero $H_{\text{int}}$, which reflects in the increase of its frequency. On increasing the applied field above $H = 100$ Oe, these two azimuthal modes merge into a mode with different spatial profile, shown in figure 4, whose frequency slightly decreases as a function of $H$, being largely localized in the lower portion of the ring.

It is noteworthy that the low-frequency mode, labelled Loc in figures 3 and 4, has a negative field dependence. At $H = 0$ Oe its profile is very similar to that of the azimuthal $(4, 0)$ mode, with the difference that it does not have a horizontal mirror plane and it is strongly localized, i.e. its dynamic magnetization oscillates close to the ring corners, being null elsewhere, in contrast to a $(4, 0)$ mode, which oscillates in the whole element. Interestingly, when $H$ is increased the minima at points B and C disappear because the field forces the magnetization to be parallel to it, while more pronounced wells are established near A and D. The positions of these wells become much closer along the path DA as $H$ is increased, and the Loc mode oscillates just in those ring regions where the magnetization has very pronounced minima, so that its frequency decreases with increasing $H$. Interestingly, this mode is an example of spin excitations 'trapped' in narrow regions where the internal field is strongly inhomogeneous, in agreement with the first observation of localized modes made by Jorzick *et al* [26].

### *3.3. Vortex to onion transition ($H = 203$ Oe)*

Even more interesting is the fact that when $H$ approaches the value corresponding to the transition (about 203 Oe) the above mentioned Loc mode becomes soft, i.e. its frequency goes to zero, as seen by the calculated curve in figure 3. (The reason why the pronounced frequency minimum predicted by the calculation is not actually observed in the experiment is probably the narrow range where the softening occurs and the statistical distribution of the physical properties of the particles in the array.) The physical meaning of this behaviour can be understood looking at the mode profile in figure 4: as stated above, it is localized within the two deep minima of the internal field located in the lower half of the ring, where the magnetization inversion occurs. Actually, the simulation shows that the vortex-to-onion

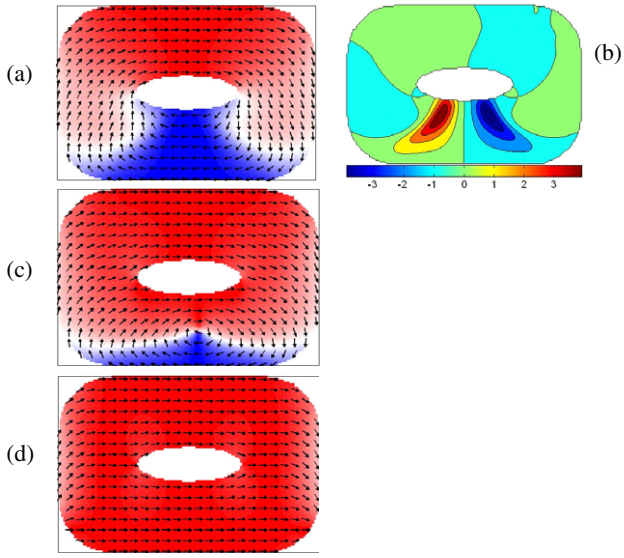


**Figure 6.** Calculated equilibrium magnetization configurations at $H = 203$ Oe (a), i.e. just before the transition from vortex to onion state, and the corresponding profile of the in-plane $y$-component (perpendicular to $H$) of the dynamic magnetization (b). (c) Snapshot of the spin configuration during the transformation. (d) Static magnetization distribution is shown at $H = 204$ Oe, i.e. after the transition.

transition takes place through the formation of a vortex (transient state) in the lower half of the ring which is suddenly expelled, attaining the final onion state. To better illustrate this point, a snapshot of the vortex transient state and of the in-plane component of the dynamical magnetization associated with the Loc mode at the transition is shown in figure 6. From these plots it is evident that the inversion of the magnetization is triggered and driven by the Loc mode, which in fact becomes soft and whose symmetry is the same as the transient state at the onset of the transition. This conclusion is in agreement with the general finding of two recent papers, where it has been found that when an abrupt magnetization switching occurs it is accompanied by a soft magnetic mode whose symmetry determines the initial steps (onset) of the microscopic reversal path [27, 28].

### *3.4. Onion state ($H > 203$ Oe)*

When $H$ is larger than 203 Oe, the magnetization is parallel to the field in all the ring portions, corresponding to the so-called onion configuration. Therefore, the spatial distribution of the modes assumes a symmetric character, reflecting the new ground state. In particular, the radial modes modify their character, evolving into DE-like modes in the saturated state, in a similar way to what was measured in circular permalloy rings [14]. The fundamental mode, instead, evolves into a mode which occupies both the long ring arms, where the internal field has its maxima. The mode coming from the merging of the (2, 0) and (4, 0) azimuthal modes assumes a mixed character (2BA $\times$ 1DE), i.e. it oscillates in both directions (parallel and perpendicular to $H$).

Concerning the lowest-frequency modes, the formerly discussed localized soft mode (Loc) disappears after the vortex-to-onion transition, but it is replaced, at low frequency, by a couple of edge modes whose spatial localization closely reflects the inhomogeneity of the internal

field (last panel of the second row in figure 4). One of the modes, labelled EXT-EM in figures 3 and 4, exhibits very pronounced oscillation at the external edges of the ring, while the other mode, labelled INT-EM, is instead localized in two symmetric internal regions, close to the ring hole. We notice that both these modes have a localized character, in analogy with those previously observed in the case of rectangular dots [29, 30], and that their frequency values depend on the effective field the spins experience in different regions.

## 4. Conclusions

In this paper we have performed a combined BLS and FMR investigation of spin-wave modes in elongated permalloy rings characterized by rather wide arms. This geometrical shape causes the presence of a strong inhomogeneity of the internal field, whose spatial distribution evolves with the strength of the externally applied magnetic field. Several eigenmodes have been identified and their frequency evolution, encompassing both the vortex and onion ground state, was measured. Micromagnetic simulations enabled us to identify the modes in terms of their symmetry and of their localization in different portions of the rings, obtaining a good quantitative agreement with the measured frequencies. Evidence has been given for a localized low-frequency mode, which, as soon as the vortex configuration is distorted by the applied field, is trapped within the deep minima of the internal field. Remarkably, this localized mode has the same spatial structure as the transient state, so it becomes soft and drives the transition from the vortex to the onion state. After the transition it is replaced by couple of edge modes, which exist at either the inner or outer boundary of the ring.

## Acknowledgment

The authors thank Professor L Gammaitoni for useful discussions.

## References

[1] Kläui M, Vaz C A F, Lopez-Diaz L and Bland J A C 2003 *J. Phys.: Condens. Matter* **15** R985 and reference therein
[2] Zhu J G, Zheng Y and Prinz G A 2000 *J. Appl. Phys.* **87** 6668
[3] Zhu J-G and Zheng Y 2002 *Spin Dynamics in Confined Magnetic Structures I* (*Springer Topics in Applied Physics* vol 83) ed B Hillebrands and K Ounadjela (Berlin: Springer) p 289
[4] Imre A, Zhou L, Orlov A, Csaba G, Bernstein G H, Porod W and Metlushko V 2004 *4th IEEE Conf. on Nanotechnology* p 137
[5] Kläui M, Vaz C A F, Heyderman L J, Rudinger U and Bland J A C 2005 *J. Magn. Magn. Mater.* **290/291** 61
[6] Castaño F J, Ross C A, Frandsen C, Eilez A, Gil D, Smith H I, Redjdal M and Humphrey F B 2003 *Phys. Rev.* B **67** 184425
[7] Castaño F J, Ross C A and Eilez A 2003 *J. Phys. D: Appl. Phys.* **36** 2031
[8] Saitoh E, Kawabata M, Harii K, Miyajima H and Yamaoka T 2004 *J. Appl. Phys.* **95** 1986
[9] Mani A S, Geerpuram D, Domanowski A, Baskaran V and Metlushko V 2004 *Nanotechnology* **15** S645
[10] Adeyeye A O, Singh N and Goolaup S 2005 *J. Appl. Phys.* **98** 094301
[11] Giesen F, Podbielski J, Korn T, Steiner M, van Staa A and Grundlerb D 2005 *Appl. Phys. Lett.* **86** 112510
[12] Neudecker I, Kläui M, Perzlmaier K, Backes D, Heyderman L J, Vaz C A F, Bland J A C, Rüdiger U and Back C H 2006 *Phys. Rev. Lett.* **96** 057207
[13] Podbielski J, Giesen F and Grundler D 2006 *Phys. Rev. Lett.* **96** 167207
[14] Gubbiotti G, Madami M, Tacchi S, Carlotti G, Tanigawa H, Ono T, Giovannini L, Montoncello F and Nizzoli F 2006 *Phys. Rev. Lett.* **97** 247203
[15] Singh N, Goolaup S and Adeyeye A O 2004 *Nanotechnology* **15** 1539
[16] Barry W 1986 *IEEE Trans. Microw. Theory Tech.* **34** 80
[17] http://math.nist.gov/oommf/

[18] Carlotti G, Gazzadi G C, Gubbiotti G, Madami M, Tacchi S and Vavassori P 2006 *Thin Solid Films* **515** 739
Gubbiotti G, Madami M, Tacchi S, Carlotti G, Socino G and Okuno T 2006 *Surf. Sci.* **600** 4143
[19] Gubbiotti G, Madami M, Tacchi S, Carlotti G and Okuno T 2006 *Phys. Rev.* B **73** 144430
[20] McMichael R D and Stiles M D 2005 *J. Appl. Phys.* **97** 10J901
[21] Torres L, Finocchio G, Lopez-Diaz L, Martinez E, Carpentieri M, Consolo G and Azzerboni B 2007 *J. Appl. Phys.* **101** 053914
[22] Gubbiotti G, Carlotti G, Okuno T, Grimsditch M, Giovannini L, Montoncello F and Nizzoli F 2005 *Phys. Rev.* B **72** 184419
[23] Giovannini L, Montoncello F, Nizzoli F, Gubbiotti G, Carlotti G, Okuno T, Shinjo T and Grimsditch M 2004 *Phys. Rev.* B **70** 172404
[24] Kittel C 1948 *Phys. Rev.* **73** 155
[25] Novosad V, Fradin F Y, Roy P E, Buchanan K S, Guslienko K Yu and Bader S D 2005 *Phys. Rev.* B **72** 024455
[26] Jorzick J, Demokritov S O, Hillebrands B, Bailleul M, Fermon C, Guslienko K Y, Slavin A N, Berkov D V and Gorn N L 2002 *Phys. Rev. Lett.* **88** 047204
[27] Leaf G, Kaper H, Yan M, Novosad V, Vavassori P, Camley R E and Grimsditch M 2006 *Phys. Rev. Lett.* **96** 017201
[28] Montoncello F, Giovannini L, Nizzoli F, Vavassori P, Grimsditch M, Ono T, Gubbiotti G, Tacchi S and Carlotti G 2007 *Phys. Rev.* B **76** 024426
[29] Gubbiotti G, Conti M, Carlotti G, Candeloro P, Di Fabrizio E, Guslienko K Yu, Andre A, Bayer C and Slavin A N 2004 *J. Phys.: Condens. Matter* **16** 7709
[30] Bayer C, Jorzick J, Hillebrands B, Demokritov S O, Guslienko K Y, Berkov D V and Gorn N L 2005 *Phys. Rev.* B **72** 064427